J. Fluid Mech. (1996), vol. 325, pp. 195–218

Wave-induced boundary layer flows above and in a permeable bed

By PHILIP L.-F. LIU, MATTHEW H. DAVIS AND SEAN DOWNING

School of Civil and Environmental Engineering, Cornell University, Ithaca, NY 14853, USA

(Received 20 January 1996 and in revised form 1 May 1996)

In this paper, the oscillatory and steady streaming velocities over a permeable bed are studied both theoretically and experimentally. Three different sizes of glass beads are used to construct permeable beds in laboratory experiments: the diameters of the glass beads are 0.5 mm, 1.5 mm, and 3.0 mm, respectively. Several experiments are performed using different wave parameters. A one-component laser-doppler velocimeter (LDV) is used to measure the horizontal velocity component inside the Stokes boundary layer above the solid and permeable surfaces. It is observed that neither oscillatory nor steady velocity components vanish on the permeable surface. The 'slip velocities' increase with increasing permeability. Based on the laminar flow assumption and the order of magnitude of the parameters used in the experiments, a perturbation theory is developed for the oscillatory velocity and the steady wave-induced streaming in the boundary layers above and inside the permeable bed. The theory confirms many experimental observations. The theory also provides the damping rate and the phase changes caused by the permeable bed.

1. Introduction

Water-wave-induced boundary layer flows above a smooth and solid surface are well-known (e.g. Batchelor 1967). For a progressive wave train with amplitude a, wavenumber k^*, and frequency ω propagating in the positive x^*-direction over a constant depth, h^*, the leading-order horizontal velocity inside the Stokes bottom boundary layer can be expressed as

$$u^* = \frac{\omega a}{\sinh k^* h^*}\left[1 - e^{-(1-i)\zeta/\sqrt{2}}\right] e^{i(k^* x^* - \omega t^*)}, \tag{1a}$$

in which ζ is the stretched boundary layer coordinate and is normalized by the boundary layer thickness, $\delta = (\nu/\omega)^{1/2}$, where ν is the kinematic viscosity of the water. Stokes (1847) pointed out that individual fluid particles in a sinusoidal, irrotational progressive wave do not describe exactly closed paths. Besides, from their orbital motions, fluid particles also process a small mean velocity in the direction of wave propagation. In a classic paper, Longuet-Higgins (1953) presented analytical solutions for the wave-induced streaming inside the bottom boundary layer under different wave fields. For a progressive wave train the wave-induced streaming inside the Stokes' boundary layer can be written as

$$(u_E^*)_{L.H.} = \frac{k^* a^2 \omega}{4 \sinh^2 k^* h^*}\left[3 - 4e^{-\zeta/\sqrt{2}} \cos\left(\frac{\zeta}{\sqrt{2}}\right) + e^{-\sqrt{2}\zeta}\right]. \tag{1b}$$

Although for a small-amplitude wave the mean drift is a second-order quantity in terms of the wave slope, k^*a, this steady current is responsible for transporting sediments and heavy pollutants near the ocean floor.

The effects of a permeable bed on the flow field above and inside the bed have been examined by many researchers using different approaches. Putnam (1949) and Reid & Kajiura (1957) investigated the wave-induced flow motions in the permeable bed and their contribution to the wave damping. In their study the flow motions inside the permeable bed are assumed to obey Darcy's law and the inviscid, irrotational flow model is used for wave motions above the permeable bed. The order of magnitude of Darcy's flow velocity inside the permeable bed is $O(\omega a(K\omega/\nu))$, in which K is the permeability in the permeable bed. Since the kinematic viscosity of water is of the order of magnitude of 10^{-6} m^2 s^{-1} and the typical value for the permeability of sandy material is of 10^{-9} m^2, the permeability parameter, $K\omega/\nu$, is of the order of 10^{-3} for a typical 10 s swell. Thus, Darcy's velocity in the permeable bed is usually much smaller than the leading-order wave velocity above the permeable bed, which is of $O(\omega a)$. Consequently, the velocity field is discontinuous along the permeable surface in both Putnam's and Reid & Kajiura's theories. Liu (1973) overcame the problem by introducing a Stokes boundary layer above the permeable surface, while Darcy's flow assumption was still used in the permeable bed. In the general derivations of governing equations for non-uniform flows in porous media, Dagan (1979) and others (e.g. Tam 1969; Lundgren 1972; Howells 1974) have concluded that Darcy's law, in which the effects of the solids in the porous medium on the mean flow is represented as the volume forces proportional linearly to the mean velocity, is valid when the scale of the mean flow variations is larger than the mean spacing between solids in the porous medium. The thickness of the Stokes boundary layer, δ, above the permeable surface is of the order of magnitude of 2 mm for a 10 s swell and 0.5 mm for a 1 s wave in laboratory experiments. Therefore, the mean flow in the porous medium must also vary drastically within a small distance from the permeable boundary, in which the shear stress becomes important (Liu & Dalrymple 1984). For simplicity, in both Liu's (1973) and Liu & Dalrymple's (1984) work the dimensionless permeability parameter, $K\omega/\nu$, has been assumed to be an order one quantity.

Based on Liu's (1973) leading-order boundary layer theory, Liu (1977) and Sleath (1978) extended Longuet-Higgins' theory to examine the effects of permeability on the wave-induced streaming. By assuming that the flow inside the porous bed is governed by Darcy's law, the wave-induced streaming in the Stokes boundary layer can be expressed as (Sleath 1978; Downing 1993)

$$u_E^* = (u_E^*)_{L.H.} + \frac{k^* a^2 \omega}{4 \sinh^2 k^* h^*} \left(\frac{\sqrt{2}}{k^* \delta} \frac{K\omega}{\nu} \right) \left[1 - e^{-\zeta/\sqrt{2}} \left(\cos \frac{\zeta}{\sqrt{2}} - \sin \frac{\zeta}{\sqrt{2}} \right) \right], \quad (2)$$

in which the porous bed has been assumed to have an infinite thickness. The wave-induced streaming consists of the solution obtained by Longuet-Higgins for the solid boundary and the contribution from the permeable bed, which could be quite significant if the ratio between the permeability parameter and the dimensionless Stokes boundary layer thickness, $k^*\delta$, becomes large. However, the shortcoming of the theory is that since Darcy's law is employed, the wave-induced streaming is always zero in the permeable bed.

Many laboratory experiments have been performed to measure wave-induced flow motions in the water column above a solid bed. In the earlier work dye tracing techniques were used to measure the mass transport velocity (e.g. Russell & Osorio

1958; Carter, Liu & Mei 1973). Because of the lack of accuracy, the velocity profile inside the bottom boundary layer cannot be resolved and only the velocity at the outer edge of the boundary layer is usually presented. More recently laser-doppler velocimeters (LDV) and hot-film anemometers have been employed to measure the velocity inside the boundary layer (e.g. Beech 1978; Sleath 1984; Hwung & Lin 1990). However, no experiment has been reported for measuring flow motions in the boundary layer over a permeable bed.

In this paper we re-examine the wave-induced flows over a permeable bed both theoretically and experimentally. A set of experimental data for the oscillatory flow motions and wave-induced streaming in the boundary layer over a permeable bed was taken with a one-component LDV. The accuracy of these measurements was first verified by comparing the data for the first-order velocity as well as the induced streaming over a solid bed with Longuet-Higgins' theoretical solutions. The measurements over porous beds were compared with the theory developed in this paper. The new theory is based on a boundary layer approach. Two boundary layers are introduced adjacent to the permeable surface, one above and the other beneath it. Perturbation solutions are obtained based on three small parameters: the wave slope, the viscous boundary layer thickness, and the permeability parameter ($K\omega/\nu$). The agreement between the experimental data and the theoretical solutions for the oscillatory motions is very good. However, it is less satisfactory for the wave-induced streaming. Several possible explanations for the discrepancies are given. From the theory the wave damping due to percolation and viscous boundary layer is also obtained.

This paper is organized in the following manner. The set-up and the procedures of laboratory experiments are discussed first. The laboratory data for the velocity inside the Stokes boundary layer over a smooth solid boundary are presented and compared with theories in this section. In § 3 a perturbation theory is developed for the oscillatory and the wave-induced streaming velocities adjacent to the permeable surface. Theoretical results are discussed in terms of the permeability parameters, $K\omega/\nu$ and γ/K. The comparisons between the experimental data and theoretical results are presented in § 4. The concluding remarks section includes a brief discussion on the relationship between Beavers & Joseph's (1967) empirical slip boundary condition and our analytical solution.

2. Experimental set-up and procedures

Laboratory experiments were performed in a wave tank which is 36 m long and 0.6 m wide. The tank has two glass sidewalls and the floor of the tank is made of sheet steel. In the middle of the tank the floor is removable. For the permeable-bed study a 1.82 m long section of the floor was removed and a false bottom was installed 0.335 m below the true bottom of the tank. Three different permeable beds were created in the trench with glass beads of different sizes: 0.5 mm, 1.5 mm and 3.0 mm in diameter.

A piston-type wavemaker at one end of the tank is controlled hydraulically by a servo-system. The wavemaker has a built-in function generator, which can provide sinusoidal signals from 0.01 Hz to 10 Hz. A one-component LDV was used to measure the horizontal velocity component inside the bottom boundary layer. The measurement volume of the LDV is an ellipsoid measuring about 30 μm along the minor axis and 150 μm along the major axis; these dimensions provide sufficient resolution of the boundary layer, whose thickness is typically 600–800 μm. The

Exp.	a (cm)	h^* (cm)	ω (s^{-1})	k^*h^*	k^*a
S1	1.25	19.1	3.77	0.55	0.036
S2	1.77	20.8	4.08	0.63	0.054
S3	1.76	35.6	3.77	0.78	0.039
S4	2.00	35.4	4.21	0.90	0.051
S5	1.63	35.9	4.71	1.04	0.047
S6	1.46	24.6	6.28	1.19	0.071

TABLE 1. Physical conditions and dimensionless parameters for experiments over a solid bottom.

sampling rate can be varied from 100 Hz to 125 Hz. Typically, 10 to 50 wave cycles are recorded at each measurement point.

Two sets of experiments were performed. The first set measured the velocities inside the Stokes boundary layer above a smooth, solid bottom. The primary purpose of this set of experiments is to make sure that the LDV system and the data analysis procedure are accurate, since analytical solutions are available. The second set of experiments measured the velocities inside the boundary layer above a permeable bed. For the solid-bottom case, six experiments were performed with k^*h^* ranging from 0.55 to 1.19. For the permeable-bed case, nine experiments with $k^*h^* = 0.78$ to 1.14 were carried out. The corresponding wavelength ranges from 1.1 m to 1.6 m. Therefore, the length of the porous bed is always longer than one wavelength.

As a summary of these experiments, table 1 shows the physical characteristics of all experiments made over the solid bottom. Table 2 lists physical characteristics of the experiments over porous beds. The Reynolds numbers, defined as $Re = u_\infty^2/\nu\omega$ where $u_\infty = a\omega/\sinh k^*h^*$ is the velocity at the outer edge of the boundary layer, are less than 1720 for the solid-bottom cases and 431 for the porous-bed cases. Therefore, the effects of turbulence are insignificant in all experiments. This has also been confirmed by our observations using dye particles. In table 2 K represents the permeability of the porous materials used in the experiments and was measured by using a constant-head permeameter (see Davis 1995). The permeameter basically consists of two constant-head tanks connected by a tube which is filled with the porous materials to be tested. By maintaining a constant-head difference in the head tanks, Δh, a constant flow rate, Q, is measured. Denoting A and L as the cross-sectional area and the length of the test tube, respectively, the permeability K is determined from Darcy's law:

$$K = \frac{\nu}{g}\frac{QL}{A\Delta h}.$$

The parameter γ appearing in table 2 is related to the diameter of the glass beads, D, as follows (Dagan 1979):

$$\gamma = \frac{D^2}{80}. \tag{3}$$

The significance of this parameter will be explained in the next section.

The LDV data were put through a coarse filter which detects the occurrences of signal 'drop-outs' (where the velocity drops to nearly zero) and 'levels' (where the velocity 'hangs' at one level for between one to five subsequent measurements), and either replaces the measurement with an interpolated value or eliminates the measurement altogether (cf. Skjelbreia 1987, for a filter designed for major data gaps due to air entrainment in breaking waves). Signal drop-outs and levels occur when the measurement volume is very close to the bottom and the light scattered

Exp.	D (mm)	h^* (cm)	ω (s^{-1})	a (cm)	K ($10^{-9}m^2$)	γ ($10^{-9}m^2$)
A2	0.5	19.9	5.01	0.517	0.235	3.13
A3	1.5	19.9	5.01	0.512	1.800	28.13
A4	3.0	19.9	5.01	0.515	7.450	112.50
B2	0.5	24.0	5.64	0.537	0.235	3.13
B3	1.5	24.0	5.64	0.513	1.800	28.13
B4	3.0	24.0	5.63	0.522	7.450	112.50
C2	0.5	24.7	6.07	1.181	0.235	3.13
C3	1.5	24.7	6.08	1.167	1.800	28.13
C4	3.0	24.7	6.07	1.140	7.450	112.50

TABLE 2. Physical conditions for experiments over a permeable bottom.

by the bottom mixes with the desired signal from the particle moving through the measurement volume. To find the oscillatory and mean velocity components from the LDV measurements, the velocity data were fitted to a multi-harmonic sinusoidal time series model with arbitrary phases, amplitudes, and the steady component. The frequency was determined beforehand from a time analysis of the velocity record. For all experiments the second harmonics were almost always less than 5% of the first harmonic and the third harmonic was typically less than 1%. The steady velocity component was obtained by the phase-averaging method.

The experimental results over a solid bottom are summarized in figures 1 and 2. The measured magnitudes of the first-harmonic velocity inside the boundary layer are plotted in figure 1. The velocity has been normalized by the free-stream velocity at the outer edge of the boundary layer. The solid line in the same figure represents the theoretical boundary layer solution, (1*a*), and is normalized by $u_\infty = a\omega/\sinh k^*h^*$. The agreement between the theory and experimental data is excellent. The wave-induced streaming velocity inside the boundary layer is plotted in figure 2; the velocity has been normalized by $k^*a^2\omega/\sinh^2 k^*h^*$. The theoretical curve is based on Longuet-Higgins' solution, i.e. (1*b*). The agreement between the laboratory data and the theoretical result is reasonable near the bottom, $\zeta < 1.0$. Large discrepancies near the outer edge of the boundary layer could be caused by the lack of consideration of weak reflection from the beach, which is less than 10%, and by the existence of a secondary current in the wave tank (Downing 1993). Sleath (1972) has also pointed out that the higher-order (nonlinearity) effects might increase or decrease mass transport significantly, depending on kh values.

The laboratory data for the permeable bed cases will be presented in §4 in conjunction with the new theory to be developed in the following section.

3. Theory

Consider a small-amplitude progressive wave train propagating over a permeable bed. The water depth is h^* and the thickness of the permeable bed is d^*. The governing equations for flow motions above the permeable bed are the well-known Navier–Stokes equations:

$$\frac{\partial \boldsymbol{u}^{+*}}{\partial t^*} + \boldsymbol{u}^{+*}\cdot\nabla\boldsymbol{u}^{+*} = -\frac{1}{\rho}\nabla p^{+*} + \nu\nabla^2\boldsymbol{u}^{+*}, \tag{4}$$

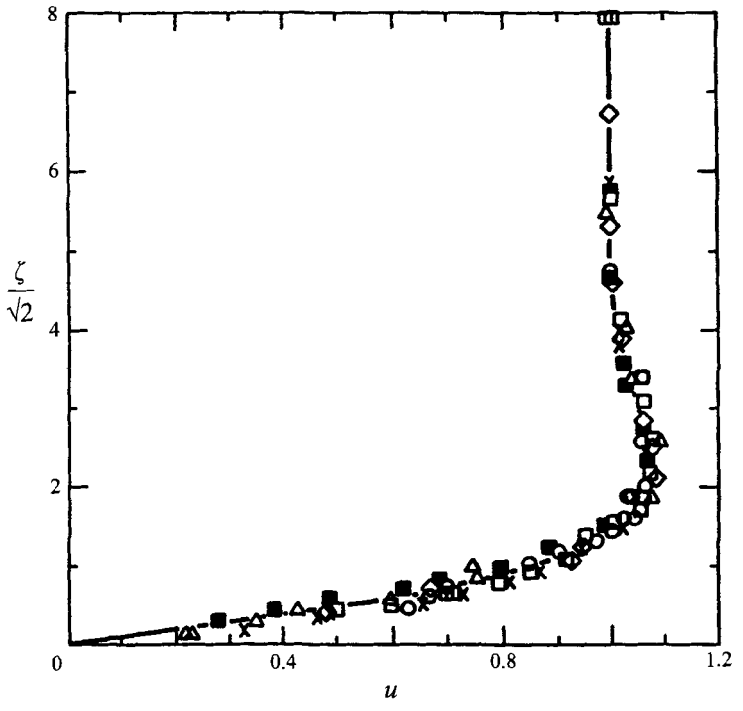

FIGURE 1. Comparison between the theory and experimental data for the magnitude of oscillatory velocity inside the Stokes boundary layer. The theoretical curve is the dimensionless version of (1*a*); the normalization factor is $\omega a/\sinh k^* h^*$. For the experimental data: ■, $kh = 0.55$; ○, $kh = 0.63$; ×, $kh = 0.78$; △, $kh = 0.90$; □, $kh = 1.04$; ◇, $kh = 1.19$.

$$\nabla \cdot \boldsymbol{u}^{+*} = 0, \tag{5}$$

in which $\boldsymbol{u}^{+*}$ denotes the velocity vector on the vertical plane, p^{+*} the pressure, ρ the density of fluid, and ν the kinematic viscosity of fluid. On the other hand, the flow in the permeable bed can be described by the following equations (e.g. Brinkman 1947; Batchelor 1974; Dagan 1979):

$$\frac{1}{n}\left\{\frac{\partial \boldsymbol{u}^{-*}}{\partial t^*} + \boldsymbol{u}^{-*} \cdot \nabla \boldsymbol{u}^{-*}\right\} = -\frac{1}{\rho}\nabla p^{-*} - \frac{\nu}{K}\boldsymbol{u}^{-*} + \frac{\nu\gamma}{K}\nabla^2 \boldsymbol{u}^{-*}, \tag{6}$$

$$\nabla \cdot \boldsymbol{u}^{-*} = 0, \tag{7}$$

where $\boldsymbol{u}^{-*}$, n, K represent the seepage velocity, the porosity, and the permeability, respectively, in the permeable bed. Equation (6) is the momentum equation for the mean fluid flow in a porous medium. The left-hand-side terms denote the acceleration per unit mass (or the inertia force per unit mass), while the right-hand-side terms represent the total forces per unit mass. The first term is the force caused by the pressure gradient. The second term denotes the effect of fixed solid particles, which is equivalent to a volume force on the fluid that is proportional to the 'local' mean fluid velocity, exactly as in Darcy's law for a porous medium (Batchelor 1974). The last term on the right-hand side represents the viscous forces and γ is a parameter depending only on the solid matrix of the permeable bed. For a very slow flow or a low Reynolds number flow, the inertia forces can be neglected. Furthermore, if the viscous term is also ignored, the momentum equation (6) reduces to the well-known Darcy's flow equation. It should be reiterated here that Darcy's law is valid if the scale

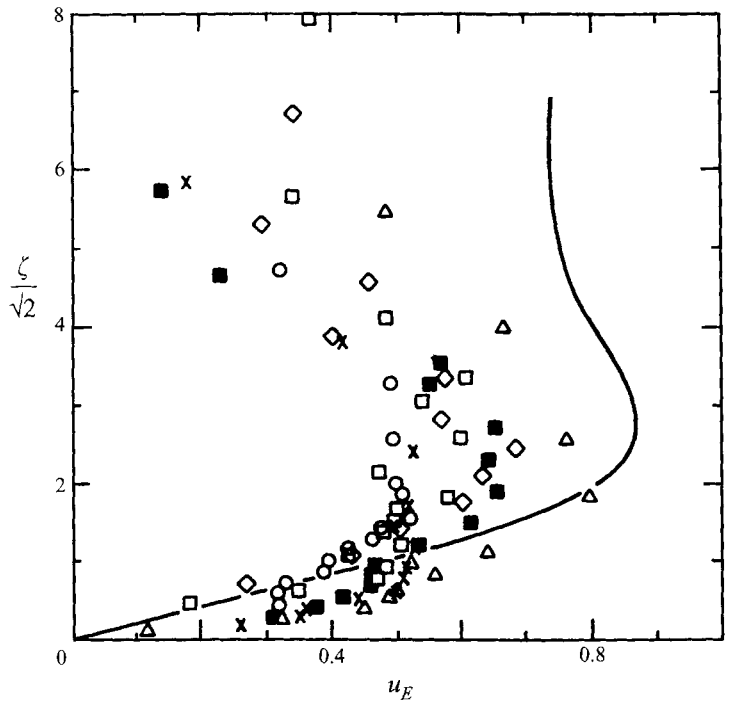

FIGURE 2. Comparison between the theory and experimental data for wave-induced steady velocity inside the Stokes' boundary layer. The theoretical curve is the dimensionless version of (1*b*); the normalization factor is $\omega k^* a^2/\sinh^2 k^* h^*$. For the experimental data: ■, $kh = 0.55$; ○, $kh = 0.63$; ×, $kh = 0.78$; △, $kh = 0.90$; □, $kh = 1.04$; ◇, $kh = 1.19$.

on which the mean velocity varies is larger than the mean spacing between the fixed solids in the porous medium (Batchelor 1974). Therefore, Darcy's equation becomes inadequate to describe the mean flow motion in the region in which the velocity varies drastically, such as the boundary layer region (Dagan 1979). More specifically, Darcy's law is unable to transfer viscous shear force from the free flow above the porous bed into the interior of the flow in the permeable bed and leads to the incorrect conclusion that the mean velocity is always zero in the porous bed. Hence, both inertia and viscous terms are considered in this paper. Rigorous derivations of (6) for a Stokes flow (i.e. ignoring the inertia term) have been given by Tam (1969), Lundgren (1972), Howells (1974), and Dagan (1979). Since spherical glass beads were used in the experiments, the γ value can be calculated by the cell model of Happel & Brenner (1965) and is related to the diameter of the glass bead, D, in the form shown in (3) (Dagan 1979).

For the progressive wave with a characteristic amplitude a and frequency, ω, the following dimensionless variables will be used in the analysis:

$$\left.\begin{aligned}(x,z,h,d) = \frac{\omega^2}{g}(x^*,z^*,h^*,d^*),\quad t = \omega t^*,\quad (\boldsymbol{u}^+,\boldsymbol{u}^-) = \frac{1}{\omega a}(\boldsymbol{u}^{+*},\boldsymbol{u}^{-*}),\\ \eta = \frac{\eta^*}{a},\quad k = \frac{g}{\omega^2}k^*,\quad p = \frac{p^*}{\rho g a},\end{aligned}\right\} \tag{8}$$

in which (x,z) denotes the dimensionless Cartesian coordinates, k the dimensionless wavenumber and η the dimensionless free-surface displacement. The corresponding

Exp.	$\alpha \times 10^{-2}$	$\beta \times 10^{-3}$	ϵ	$\theta \times 10^{-1}$	k_0
A2	1.32	1.18	1.14	1.25	1.532
B2	1.74	1.32	1.37	1.33	1.303
C2	4.44	1.43	1.52	1.38	1.228
A3	1.31	9.02	1.14	3.75	1.532
B3	1.66	1.02	1.37	3.98	1.303
C3	4.02	1.09	1.53	4.14	1.227
A4	1.32	3.73	1.14	7.51	1.532
B4	1.69	4.19	1.36	7.96	1.305
C4	4.28	4.52	1.52	8.26	1.228

TABLE 3. Dimensionless parameters for experiments over a permeable bottom.

dimensionless governing equations become

$$\frac{\partial \boldsymbol{u}^+}{\partial t} + \alpha \boldsymbol{u}^+ \cdot \nabla \boldsymbol{u}^+ = -\nabla p^+ + \epsilon^2 \nabla^2 \boldsymbol{u}^+, \tag{9}$$

$$\nabla \cdot \boldsymbol{u}^+ = 0, \tag{10}$$

for flow motions above the porous bed, and

$$\frac{\beta}{n}\left\{\frac{\partial \boldsymbol{u}^-}{\partial t} + \alpha \boldsymbol{u}^- \cdot \nabla \boldsymbol{u}^-\right\} = -\beta \nabla p^- - \boldsymbol{u}^- + \epsilon^2 \theta^2 \nabla^2 \boldsymbol{u}^-, \tag{11}$$

$$\nabla \cdot \boldsymbol{u}^- = 0, \tag{12}$$

for flow motions inside the permeable bed. In the above equations three parameters have been introduced:

$$\alpha = \frac{\omega^2 a}{g}, \quad \epsilon = \frac{\omega^2}{g}\left(\frac{\nu}{\omega}\right)^{1/2}, \quad \beta = \frac{K\omega}{\nu}, \tag{13}$$

in which α denotes the wave slope, ϵ measures the thickness of the viscous boundary layer relative to a characteristic wavelength, and β indicates the magnitude of seepage flows in the porous bed. Based on the experimental data presented in the previous section, these parameters are small (see table 3). On the other hand, it is important to note that the parameter

$$\theta = \left(\frac{\gamma}{K}\right)^{1/2}\left(\frac{K\omega}{\nu}\right)^{1/2}, \tag{14}$$

is an order-one quantity in most of the experiments (see table 3). Therefore, from (11), it is expected that a boundary layer of thickness of $O(\epsilon\theta)$ exists in the porous bed.

3.1. *A perturbation analysis*

The dynamics of the flow problem can be presented in the following manner. In the flow region above the permeable bed, motions are essentially irrotational except in the boundary layers adjacent to the free surface, $z = \eta$, and the permeable boundary, $z = -h$. Because the permeability of the porous bed is small, i.e. $\beta \ll 1$, for the leading-order flow problem the wave does not sense the porous bed so that the solution for irrotational motions is the same as the well-known potential flow solution for small-amplitude waves over a solid bottom. However, the hydrodynamic pressure on the permeable surface, $z = -h$, induces Darcy-type flow

motions inside the porous bed, which are of the order of magnitude of β. At the same time, a leading-order horizontal rotational velocity component is generated inside the boundary layers above and underneath the permeable surface in order to satisfy the continuity of the horizontal velocity component and its vertical derivative across the permeable surface at the leading order. Since the Darcy-type flow motions give a finite velocity, in both horizontal and vertical directions, on the permeable surface, both irrotational and rotational flow motions above the permeable bed must be corrected at order β. By integrating the leading-order continuity equation inside the boundary layers, one finds that a vertical velocity component of order ϵ is generated. Therefore, the irrotational and rotational velocity inside the boundary layers must also be corrected at order ϵ. Finally, at order α, wave-induced streaming inside the boundary layers generated by the nonlinear interactions among the lower-order velocity components (i.e. Reynolds stresses induced by wave motions).

Accordingly, we now introduce the following perturbation expansions. Since there are two additional horizontal length scales due to viscous damping and percolation, $O(1/k\epsilon)$ and $O(1/k\beta)$, respectively, in additional to the wavelength, $O(1/k)$, we shall expand the dimensionless k in powers of ϵ and β. Thus,

$$\boldsymbol{u}^{+} = \nabla[(\phi_0 + \beta\phi_{11} + \epsilon\phi_{10})e^{i(kx-t)}] + [\boldsymbol{u}_0^{+r} + \beta\boldsymbol{u}_{11}^{+r} + \epsilon\boldsymbol{u}_{10}^{+r}]e^{i(kx-t)} + \alpha\boldsymbol{u}_{01}^{+} + \cdots, \quad (15a)$$

$$\boldsymbol{u}^{-} = [\boldsymbol{u}_0^{-r} + \beta(\boldsymbol{u}_{11}^{-D} + \boldsymbol{u}_{11}^{r}) + \epsilon\boldsymbol{u}_{10}^{-r}]e^{i(kx-t)} + \alpha\boldsymbol{u}_{01}^{-} + \cdots, \quad (15b)$$

$$p^{\pm} = [p_0^{\pm} + \beta p_{11}^{\pm} + \epsilon p_{10}^{\pm}]e^{i(kx-t)} + \alpha p_{01}^{\pm} + \cdots, \quad (15c)$$

$$\eta = (\eta_0 + \beta\eta_{11} + \epsilon\eta_{10})e^{i(kx-t)} + \alpha\eta_{01} + \cdots, \quad (15d)$$

$$k = k_0 + \beta k_{11} + \epsilon k_{10} + \cdots, \quad (15e)$$

in which the velocity in the flow region above the porous bed, up to $O(\epsilon)$, has been decomposed into irrotational and rotational components. While the rotational components, with a superscript r in (15*a*,*b*), exist only in the boundary layers, the velocity potential satisfies the Laplace equation,

$$\nabla^2(\phi e^{i(kx-t)}) = 0, \quad (16)$$

in which ϕ could be ϕ_0, ϕ_{11}, or ϕ_{10}, in the entire flow domain above the porous bed so that the continuity equation is satisfied. The boundary layer adjacent to the permeable surface has a thickness of $O(\epsilon)$. By adopting the stretched coordinate

$$\zeta = \frac{z + h}{\epsilon}, \quad (17)$$

the continuity equation for the rotational velocity in the boundary layer becomes

$$\frac{\partial u^{r+}}{\partial x} + \frac{1}{\epsilon}\frac{\partial w^{r+}}{\partial \zeta} = 0, \quad (18)$$

in which (u^{r+}, w^{r+}) are the rotational velocity components. In the boundary layer the momentum equation, (9), can be expressed in the following component form:

$$\frac{\partial u^{+}}{\partial t} + \alpha\left(u^{+}\frac{\partial u^{+}}{\partial x} + \frac{w^{+}}{\epsilon}\frac{\partial u^{+}}{\partial \zeta}\right) = -\frac{\partial p^{+}}{\partial x} + \frac{\partial^2 u^{+}}{\partial \zeta^2} + O(\epsilon^2), \quad (19a)$$

$$\frac{\partial w^{+}}{\partial t} + \alpha\left(u^{+}\frac{\partial w^{+}}{\partial x} + \frac{w^{+}}{\epsilon}\frac{\partial w^{+}}{\partial \zeta}\right) = -\frac{\partial p^{+}}{\partial z} + \frac{\partial^2 w^{+}}{\partial \zeta^2} + O(\epsilon^2). \quad (19b)$$

We remark here that a boundary layer with the same thickness, $O(\epsilon)$, also exists adjacent to the free surface. However, the leading rotational velocity in the free-surface boundary layer is of $O(\epsilon)$ (e.g. Batchelor 1967) and will not affect the analysis for flow motions in the bottom boundary layer, up to $O(\alpha)$. Therefore, we will not discuss the free-surface boundary layer in this paper.

Underneath the permeable surface a boundary layer with the stretched coordinate

$$\xi = -\frac{z+h}{\epsilon\theta}, \tag{20}$$

exists, within which the momentum equations are written as

$$\frac{\beta}{n}\left[\frac{\partial u^-}{\partial t} + \alpha\left(u^-\frac{\partial u^-}{\partial x} - \frac{w^-}{\epsilon\theta}\frac{\partial u^-}{\partial \xi}\right)\right] = -\beta\frac{\partial p^-}{\partial x} - u^- + \frac{\partial^2 u^-}{\partial \xi^2} + O(\epsilon^2), \tag{21a}$$

$$\frac{\beta}{n}\left[\frac{\partial w^-}{\partial t} + \alpha\left(u^-\frac{\partial w^-}{\partial x} - \frac{w^-}{\epsilon\theta}\frac{\partial w^-}{\partial \xi}\right)\right] = -\beta\frac{\partial p^-}{\partial z} - w^- + \frac{\partial^2 w^-}{\partial \xi^2} + O(\epsilon^2), \tag{21b}$$

$$\frac{\partial u^-}{\partial x} - \frac{1}{\epsilon\theta}\frac{\partial w^-}{\partial \xi} = 0. \tag{21c}$$

The boundary layer thickness is $O(\epsilon\theta)$, with θ being $O(1)$. Outside the boundary layer, the flow motion is governed by Darcy's law, i.e.

$$u^- = -\beta\frac{\partial p^-}{\partial x}, \quad w^- = -\beta\frac{\partial p^-}{\partial z}. \tag{22a}$$

From the continuity equation, the pressure field satisfies the Laplace equation,

$$\nabla^2 p^- = 0. \tag{22b}$$

The boundary conditions can be summarized as follows. On the free surface the kinematic and dynamic boundary conditions can be approximately written as

$$\frac{\partial \eta}{\partial t} = \frac{\partial \phi}{\partial z} \text{ on } z = 0, \tag{23a}$$

$$\frac{\partial \phi}{\partial t} + \eta = 0 \text{ on } z = 0. \tag{23b}$$

Along the permeable surface, $z = -h$, the velocity and the vertical derivative of the horizontal velocity component are required to be continuous. Finally the velocity vanishes along the bottom of the porous bed, $z = -(h+d)$. We remark here that a boundary layer of thickness $O(\epsilon\theta)$ appears next to the solid surface, $z = -(h+d)$. However, the leading-order velocity in this boundary layer is of $O(\beta)$, and will not affect the results in the boundary layers near the permeable surface. Therefore, the results for the solid-surface boundary layer will not be presented in the present analysis.

When (15) are substituted into (16)–(23) and orders are separated, a sequence of problems is obtained.

(i) Inviscid solution at $O(1)$:

$$\left(\frac{\mathrm{d}^2}{\mathrm{d}z^2} - k_0^2\right)\phi_0 = 0, \quad -h < z < 0. \tag{24a}$$

$$\frac{\mathrm{d}\phi_0}{\mathrm{d}z} = 0, \quad z = -h, \tag{24b}$$

$$\frac{\mathrm{d}\phi_0}{\mathrm{d}z} - \phi_0 = 0, \quad z = 0, \tag{24c}$$

$$\eta_0 = \mathrm{i}\phi_0, \quad z = 0. \tag{24d}$$

The leading-order problem describes a progressive wave train over a solid bottom. The solution is well-known and can be written as

$$\phi_0 = -\mathrm{i}\frac{\cosh k_0(z+h)}{\cosh k_0 h}, \tag{25a}$$

$$\eta_0 = 1, \tag{25b}$$

with the dispersion relationship

$$k_0 \tanh k_0 h = 1. \tag{26}$$

The corresponding dynamic pressure is

$$p_0^+ = \mathrm{i}\phi_0 = \frac{\cosh k_0(z+h)}{\cosh k_0 h}, \tag{27a}$$

which has a finite value along the bottom, $z = -h$,

$$p_0^+|_{z=-h} = \frac{1}{\cosh k_0 h}, \tag{27b}$$

and it, in turn, generates Darcy-type flow motions in the porous bed at $O(\beta)$.

From (25*a*), one finds that the vertical velocity component vanishes at the bottom, while the horizontal velocity component remains a constant, i.e.

$$\mathrm{i}k_0\phi_0|_{z=-h} = \frac{k_0}{\cosh k_0 h}, \tag{28}$$

which suggests that $O(1)$ boundary layer solutions are required to satisfy the continuity of the velocity along the permeable surface.

(ii) Boundary layer corrections of $O(1)$:

In the boundary layer above the permeable surface, $\zeta > 0$, the rotational velocity component satisfies the following equations:

$$-\mathrm{i}u_0^{+r} = \frac{\mathrm{d}^2 u_0^{+r}}{\mathrm{d}\zeta^2}, \tag{29a}$$

$$u_0^{+r} \to 0, \quad \zeta \to \infty. \tag{29b}$$

Similarly, in the boundary layer underneath the permeable surface, $\xi > 0$, the horizontal velocity component is the solution of the following equations:

$$\frac{\mathrm{d}^2 u_0^{-r}}{\mathrm{d}\xi^2} - u_0^{-r} = 0, \tag{30a}$$

$$u_0^{-r} \to 0, \quad \xi \to \infty. \tag{30b}$$

The continuity of the $O(1)$ horizontal velocity component and its vertical derivative requires the following conditions:

$$\mathrm{i}k_0\phi_0|_{z=-h} + u_0^{+r}|_{\zeta=0} = u_0^{-r}|_{\xi=0}, \tag{31a}$$

$$\left.\frac{\mathrm{d}u_0^{+r}}{\mathrm{d}z}\right|_{\zeta=0} = \left.\frac{\mathrm{d}u_0^{-r}}{\mathrm{d}z}\right|_{\xi=0}. \tag{31b}$$

The boundary layer solutions can be readily obtained as

$$u_0^{+r} = Be^{-(1-i)\zeta/\sqrt{2}}, \tag{32a}$$

$$u_0^{-r} = Ce^{-\xi}, \tag{32b}$$

with

$$B = -\frac{k_0}{\cosh k_0 h}\left\{1 + \frac{1-i}{\sqrt{2}}\theta\right\}^{-1}, \tag{32c}$$

$$C = -\frac{1-i}{\sqrt{2}}\theta B. \tag{32d}$$

The solution, (32), implies that while the phase of the horizontal velocity changes continuously throughout the boundary layer above the permeable surface, it remains a constant in the boundary layer in the porous bed.

The continuity equations give

$$ik_0 u_0^{+r} + \frac{dw_{10}^{+r}}{d\zeta} = 0, \tag{33a}$$

$$ik_0 u_0^{-r} - \frac{1}{\theta}\frac{dw_{10}^{-r}}{d\xi} = 0, \tag{33b}$$

from which the $O(\epsilon)$ vertical velocity components inside the boundary layers may be integrated from outside the boundary (i.e. $\zeta \to \infty$ and $\xi \to \infty$) inward to ζ and ξ, respectively. Thus,

$$w_{10}^{+r} = \frac{(i-1)k_0 B}{\sqrt{2}}e^{-(1-i)\zeta/\sqrt{2}}, \tag{34a}$$

$$w_{10}^{-r} = -ik_0\theta C e^{-\xi}. \tag{34b}$$

Because w_{10}^{+r} and w_{10}^{-r} are not the same on the permeable surface ($\zeta = 0$ and $\xi = 0$), the difference must be balanced by the irrotational velocity component $d\phi_{10}/dz$ at $O(\epsilon)$.

(iii) Darcy's solution of $O(\beta)$:

In this order of magnitude, the velocity components are determined by the pressure gradient. Thus

$$u_{11}^{-D} = -ik_0 p_0^-, \tag{35a}$$

$$w_{11}^{-D} = -\frac{dp_0^-}{dz}. \tag{35b}$$

From the continuity equation the pressure field satisfies the following equation:

$$\frac{d^2 p_0^-}{dz^2} - k_0^2 p_0^- = 0, \quad -(h+d) < z < -h. \tag{36a}$$

The boundary conditions are

$$p_0^- = p_0^+, \quad z = -h, \tag{36b}$$

$$\frac{dp_0^-}{dz} = 0. \quad z = -(h+d). \tag{36c}$$

The solution for the pressure field can be readily obtained when (27*b*) is used in (36*b*). Thus,

$$p_0^- = \frac{\cosh k_0(z+h+d)}{\cosh k_0 d \cosh k_0 h}. \tag{37}$$

The velocity field can be calculated from (35*a*) and (35*b*), which has finite values along the permeable surface, i.e.

$$u_{11}^-|_{z=-h} = -\frac{\mathrm{i}k_0}{\cosh k_0 h}, \tag{38a}$$

$$w_{11}^-|_{z=-h} = -\frac{k_0 \tanh k_0 d}{\cosh k_0 h}. \tag{38b}$$

These velocity components must be matched by the flow field above the permeable surface at $O(\beta)$, which leads to the next problem.

(iv) Inviscid correction of $O(\beta)$:

$$\left(\frac{\mathrm{d}^2}{\mathrm{d}z^2} - k_0^2\right)\phi_{11} = 2k_0 k_{11}\phi_0, \quad -h < z < 0. \tag{39a}$$

$$\frac{\mathrm{d}\phi_{11}}{\mathrm{d}z} = w_{11}^-, \quad z = -h, \tag{39b}$$

$$\frac{\mathrm{d}\phi_{11}}{\mathrm{d}z} - \phi_{11} = 0, \quad z = 0, \tag{39c}$$

$$\eta_{11} = \mathrm{i}\phi_{11}, \quad z = 0. \tag{39d}$$

The solution may be expressed as

$$\phi_{11} = E\cosh k_0(z+h) + \left(F - \frac{\mathrm{i}k_{11}(z+h)}{\cosh k_0 h}\right)\sinh k_0(z+h), \tag{40a}$$

where

$$F = -\frac{\tanh k_0 d}{\cosh k_0 h}, \tag{40b}$$

$$k_{11} = \mathrm{i}\frac{2k_0 \tanh k_0 d}{2k_0 h + \sinh 2k_0 h}, \tag{40c}$$

$$E = \frac{\mathrm{i}k_{11} h \tanh k_0 h}{\cosh k_0 h} - F\tanh k_0 h, \tag{40d}$$

and the free-surface displacement, η_{11}, has been assumed to be zero. The expression for k_{11} is a pure imaginary constant. Therefore, it represents the damping rate caused by the percolation in the permeable bed; the percolation does not affect the phase up to this order of magnitude. As the thickness of the porous bed becomes large, $k_0 d \to \infty$, the damping rate k_{11} gives the same expression as the one derived by Reid & Kajiura (1957).

It is clear that the horizontal velocity component of the inviscid solution is non-zero on the permeable surface. Hence, corrections must be made in the boundary layers at $O(\beta)$.

(v) Boundary-layer corrections of $O(\beta)$:

In the boundary layer above the permeable surface, $\zeta > 0$, the rotational velocity

component satisfies the following equations:

$$-\mathrm{i}u_{11}^{+r} = \frac{\mathrm{d}^2 u_{11}^{+r}}{\mathrm{d}\zeta^2}, \tag{41a}$$

$$u_{11}^{+} \to 0, \quad \zeta \to \infty. \tag{41b}$$

Similarly, in the boundary layer underneath the permeable surface, $\xi > 0$, the horizontal velocity component is the solution of the following equations:

$$\frac{\mathrm{d}^2 u_{11}^{-r}}{\mathrm{d}\xi^2} - u_{11}^{-r} = \frac{-\mathrm{i}}{n} u_0^{-r}, \tag{42a}$$

$$u_{11}^{-r} \to 0, \quad \xi \to \infty. \tag{42b}$$

The continuity of the $O(\beta)$ horizontal velocity component and its vertical derivative across the permeable surface requires the following conditions:

$$(\mathrm{i}k_{11}\phi_0 + \mathrm{i}k_0\phi_{11})|_{z=-h} + u_{11}^{+r}|_{\zeta=0} = (u_{11}^{-r} + u_{11}^{-D})|_{\xi=0}, \tag{42c}$$

$$\left.\frac{\mathrm{d}u_{11}^{+r}}{\mathrm{d}z}\right|_{\zeta=0} = \left.\frac{\mathrm{d}u_{11}^{-r}}{\mathrm{d}z}\right|_{\xi=0}. \tag{42d}$$

The boundary layer solutions can be readily obtained as

$$u_{11}^{+r} = G\mathrm{e}^{-(1-i)\zeta/\sqrt{2}}, \tag{43a}$$

$$u_{11}^{-r} = \left(H + \frac{iC\xi}{2n}\right)\mathrm{e}^{-\xi}, \tag{43b}$$

with

$$H = \left(1 + \frac{1+\mathrm{i}}{\sqrt{2}\theta}\right)^{-1}\left[\mathrm{i}k_0\left(\frac{-\mathrm{i}k_{11}}{k_0\cosh k_0 h} + \frac{1}{\cosh k_0 h} + E\right) + \frac{\mathrm{i}-1}{2\sqrt{2}}\frac{C}{\theta n}\right], \tag{43c}$$

$$G = H - \mathrm{i}k_0\left(E + \frac{1}{\cosh k_0 h} - \frac{\mathrm{i}k_{11}}{k_0\cosh k_0 h}\right). \tag{43d}$$

(vi) Inviscid solution of $O(\epsilon)$

Because of the difference in w_{10}^{+r} and w_{10}^{-r} along the permeable surface, (see (34)), the irrotational velocity field must be corrected at $O(\epsilon)$ so that the continuity is satisfied along the permeable surface:

$$\left(\frac{\mathrm{d}^2}{\mathrm{d}z^2} - k_0^2\right)\phi_{10} = 2k_0 k_{10}\phi_0, \quad -h < z < 0. \tag{44a}$$

$$\frac{\mathrm{d}\phi_{10}}{\mathrm{d}z} + w_{10}^{+r} = w_{10}^{-r}, \quad z = -h, \tag{44b}$$

$$\frac{\mathrm{d}\phi_{10}}{\mathrm{d}z} - \phi_{10} = 0, \quad z = 0, \tag{44c}$$

$$\eta_{10} = \mathrm{i}\phi_{10}, \quad z = 0. \tag{44d}$$

The solution may be obtained as

$$\phi_{10} = M\cosh k_0(z+h) + \left(N - \frac{\mathrm{i}k_{10}(z+h)}{\cosh k_0 h}\right)\sinh k_0(z+h), \tag{45a}$$

where

$$N = \frac{1-\mathrm{i}}{\sqrt{2}}B - \mathrm{i}\theta C, \tag{45b}$$

$$k_{10} = \frac{\sqrt{2}k_0^2 \cosh k_0 h}{2k_0 h + \sinh 2k_0 h}(1 + \mathrm{i} - \sqrt{2}\theta), \tag{45c}$$

$$M = \frac{\mathrm{i}k_{10} \tanh k_0 h}{\cosh k_0 h} - N \tanh k_0 h, \tag{45d}$$

in which we have assumed that $\eta_{10} = 0$. The real part of the expression for k_{10} represents the phase modification, while the imaginary part represents the damping rate. Both are caused by the viscous boundary layers above and below the permeable surface. For the special case with $\gamma = 0$, k_{10} can be simplified to

$$k_{10} = (1 + \mathrm{i})\frac{\sqrt{2}k_0^2}{2k_0 h + \sinh 2k_0 h}, \tag{46}$$

which is the well-known solution for the effects of a Stokes' boundary layer over a solid bottom on the wavenumber and wave damping.

Once again, the horizontal velocity component of the inviscid solution is non-zero on the permeable surface. Hence, corrections must be made in the boundary layers at $O(\epsilon)$.

(vii) Boundary-layer corrections of $O(\epsilon)$:

In the boundary layer above the permeable surface, $\zeta > 0$, the rotational velocity component satisfies the following equations:

$$-\mathrm{i}u_{10}^{+r} = \frac{\mathrm{d}^2 u_{10}^{+r}}{\mathrm{d}\zeta^2}, \tag{47a}$$

$$u_{10}^{+r} \to 0, \quad \zeta \to \infty. \tag{47b}$$

Similarly, in the boundary layer underneath the permeable surface, $\xi > 0$, the horizontal velocity component is the solution of the following equations:

$$\frac{\mathrm{d}^2 u_{10}^{-r}}{\mathrm{d}\xi^2} - u_{10}^{-r} = 0, \tag{48a}$$

$$u_{10}^{-r} \to 0, \quad \xi \to \infty. \tag{48b}$$

The continuity of the $O(\epsilon)$ horizontal velocity component and its vertical derivative requires the following conditions:

$$(\mathrm{i}k_{10}\phi_0 + \mathrm{i}k_0\phi_{10})|_{z=-h} + u_{10}^{+r}|_{\zeta=0} = u_{10}^{-r}|_{\xi=0}, \tag{49a}$$

$$\left.\frac{\mathrm{d}u_{10}^{+r}}{\mathrm{d}z}\right|_{\zeta=0} = \left.\frac{\mathrm{d}u_{10}^{-r}}{\mathrm{d}z}\right|_{\xi=0}. \tag{49b}$$

The boundary layer solutions can be readily obtained as

$$u_{10}^{+r} = Q\mathrm{e}^{-(1-\mathrm{i})\zeta/\sqrt{2}}, \tag{50a}$$

$$u_{10}^{-r} = R\mathrm{e}^{-\xi}, \tag{50b}$$

with

$$R = \left(\frac{1+\mathrm{i}}{\sqrt{2}\theta} + 1\right)^{-1} \left(\mathrm{i}k_0 M + \frac{k_{10}}{\cosh k_0 h}\right), \tag{50c}$$

$$Q = R - \mathrm{i}k_0 M - \frac{k_{10}}{\cosh k_0 h}. \tag{50d}$$

3.2. *Wave-induced streaming*

The wave-induced streaming inside the boundary layers is of $O(\alpha)$ and is governed by the following equations:

$$\frac{\mathrm{d}^2\overline{u}_{01}^{+}}{\mathrm{d}\zeta^2} = \frac{1}{\epsilon}\overline{\frac{\mathrm{d}\phi_0}{\mathrm{d}z}\frac{\mathrm{d}u_0^{+r}}{\mathrm{d}\zeta}} + \overline{\frac{\mathrm{d}\phi_{10}}{\mathrm{d}z}\frac{\mathrm{d}u_0^{+r}}{\mathrm{d}\zeta}} + \overline{w_{10}^{+r}\frac{\mathrm{d}u_0^{+r}}{\mathrm{d}\zeta}} + \frac{\beta}{\epsilon}\overline{\frac{\mathrm{d}\phi_{11}}{\mathrm{d}z}\frac{\mathrm{d}u_0^{+r}}{\mathrm{d}\zeta}}, \tag{51a}$$

$$\frac{\mathrm{d}^2\overline{u}_{01}^{-}}{\mathrm{d}\xi^2} - \overline{u}_{01}^{-} = 0, \tag{51b}$$

in which the overbar represents the time average over a wave period. We remark here that the inviscid vertical velocity, $\mathrm{d}\phi_0/\mathrm{d}z$, is proportional to $\epsilon\zeta$ in the boundary layer (see (24*b*)). Furthermore, to include the effects of percolation we have assumed that β/ϵ is $O(1)$. Substituting (25*a*), (32*a*), (34*a*), (40*a*), and (45*a*) in (51*a*), we obtain

$$\frac{\mathrm{d}^2\overline{u}_{01}^{+}}{\mathrm{d}\zeta^2} = \tfrac{1}{2}Re\left\{k_0B^2\left[e^{-\sqrt{2}\zeta} - (1+\mathrm{i}\theta^2)\mathrm{e}^{-((1+\mathrm{i})/\sqrt{2})\zeta}\right]\right.$$

$$\left. + \frac{(\mathrm{i}-1)k_0B^*}{\sqrt{2}\cosh k_0 h}\left[k_0\zeta - \mathrm{i}\frac{\beta}{\epsilon}\tanh k_0 d\right]\mathrm{e}^{-((1+\mathrm{i})/\sqrt{2})\zeta}\right\}. \tag{52}$$

Integrating (52) and (51*b*) twice and applying the boundary conditions

$$\overline{u}_{01}^{+} = \overline{u}_{01}^{-}, \quad \zeta = 0,\ \xi = 0, \tag{53a}$$

$$\frac{\mathrm{d}\overline{u}_{01}^{+}}{\mathrm{d}z} = \frac{\mathrm{d}\overline{u}_{01}^{-}}{\mathrm{d}z}, \quad \zeta = 0,\ \xi = 0, \tag{53b}$$

$$\frac{\mathrm{d}\overline{u}_{01}^{+}}{\mathrm{d}\zeta} \to 0 \quad \zeta \to \infty, \tag{53c}$$

$$\frac{\mathrm{d}\overline{u}_{01}^{-}}{\mathrm{d}\xi} \to 0 \quad \xi \to \infty, \tag{53d}$$

we find the steady streaming in the boundary layers as follows:

$$\overline{u}_{01}^{+} = \tfrac{1}{2}\mathrm{Re}\left\{k_0B^2\left[\tfrac{1}{2}\mathrm{e}^{-\sqrt{2}\zeta} + (\mathrm{i}-\theta^2)\mathrm{e}^{-\frac{1+\mathrm{i}}{\sqrt{2}}\zeta}\right] + \frac{k_0B^*}{\cosh k_0 h}\left[\frac{k_0(1+\mathrm{i})\zeta}{\sqrt{2}}\right.\right.$$

$$\left.\left. + 2k_0 + \frac{\beta}{\epsilon}\frac{1-\mathrm{i}}{\sqrt{2}}\tanh k_0 d\right]\mathrm{e}^{-((1+\mathrm{i})/\sqrt{2})\zeta}\right\} + C_2, \tag{54a}$$

$$\overline{u}_{01}^{-} = C_3\mathrm{e}^{-\xi}, \tag{54b}$$

where

$$C_3 = \frac{1}{2}\theta\mathrm{Re}\left\{k_0B^2\left(-\frac{i}{\sqrt{2}} + \theta^2\frac{1+\mathrm{i}}{\sqrt{2}}\right) + \frac{k_0B^*}{\cosh k_0 h}\left[-k_0\frac{1+\mathrm{i}}{\sqrt{2}} - \frac{\beta}{\epsilon}\tanh k_0 d\right]\right\}, \tag{54c}$$

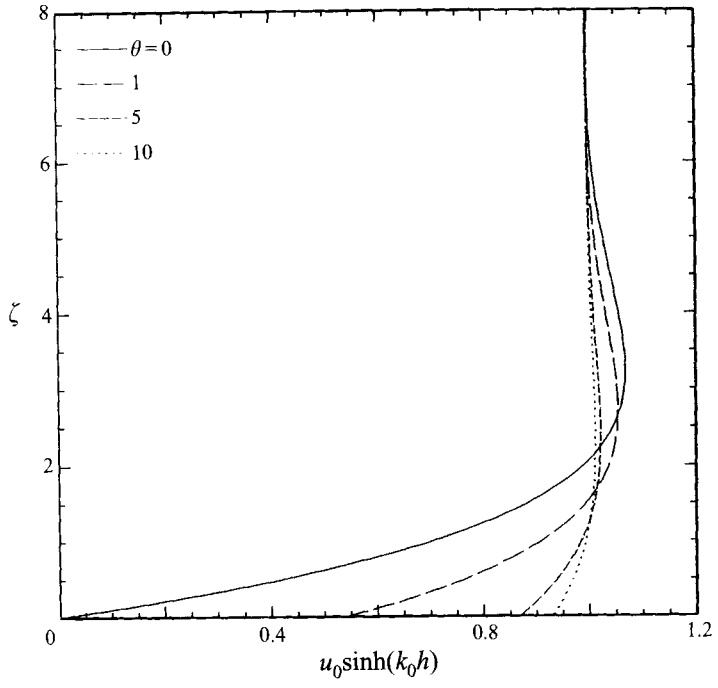

FIGURE 3. The effects of permeability parameter, θ, on the magnitude of the leading-order horizontal oscillatory velocity inside the boundary layer above the permeable surface.

$$C_2 = C_3 - \tfrac{1}{2}\mathrm{Re}\left\{k_0B^2(\tfrac{1}{2}+\mathrm{i}-\theta^2)+\frac{k_0B^*}{\cosh k_0h}\left[2k_0+\frac{\beta}{\epsilon}\frac{1-\mathrm{i}}{\sqrt{2}}\tanh k_0d\right]\right\}. \quad (54d)$$

The induced streaming at the outer edge of the boundary layer above the permeable bed is C_2. For the special case when the sea floor is a solid, impervious surface, i.e. $K = \gamma = 0$, the parameters β and θ also become zero. Hence, $C_3 = 0$ and

$$\overline{u}_{01}^{+}|_{\zeta\to\infty} = C_2 = \frac{3}{4}\frac{k_0^3}{\cosh^2 k_0h}, \quad (55)$$

which is the same as the Longuet-Higgins' solution. (The dimensional form of the above equation is the same as that given in (1*b*) as $\zeta \to \infty$.) On the other hand, when only γ is assumed to be zero, the induced streaming at the outer edge of the boundary layer becomes

$$\overline{u}_{01}^{+}|_{\zeta\to\infty} = C_2 = \frac{3}{4}\frac{k_0^3}{\cosh^2 k_0h}+\frac{\beta}{\epsilon}\frac{1}{2\sqrt{2}}\frac{\tanh k_0d}{\sinh^2 k_0h}, \quad (56)$$

in which the second term represents the effects of percolation. If the thickness of the porous bed is large in comparison with the wavelength, the above expression becomes the same as (2) for $\zeta \to \infty$.

3.3. *Discussion on analytical solutions*

In figure 3 the leading-order horizontal velocity inside the boundary layer is plotted for different values of θ. This velocity is the sum of the irrotational and rotational components. For $\theta = 0$, the case coincides with the impermeable bed case up to this order of magnitude. Therefore, the horizontal velocity vanishes at $\zeta = 0$. On the other hand, when θ is not zero, there is a slip velocity along the permeable surface,

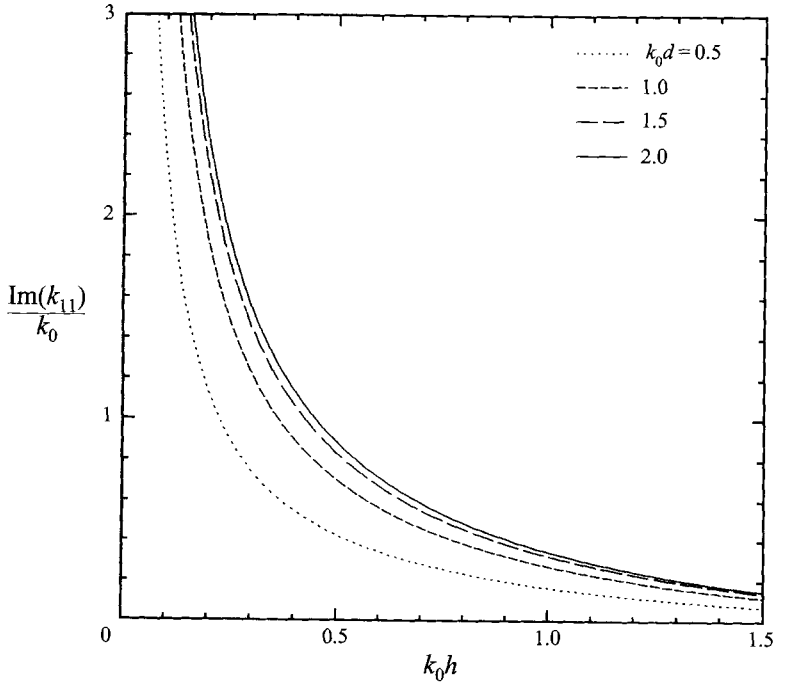

FIGURE 4. The damping rate due to percolation as a function of k_0h and k_0d.

which increases with increasing θ. The theoretical expression for the leading-order slip velocity on the permeable surface can be found from (31c) and (32), i.e.

$$u_0^{-r}|_{\xi=0} = \frac{k_0}{\cosh k_0 h} \frac{1-\mathrm{i}}{\sqrt{2}} \theta \left\{ 1 + \frac{1-\mathrm{i}}{\sqrt{2}} \theta \right\}^{-1}. \tag{57}$$

For the laboratory case the θ is of order one. The corrections to the horizontal velocity due to percolation, βu_{11}, and the higher-order viscous effect, ϵu_{10}, are insignificant, since both parameters β and ϵ are quite small. The leading-order horizontal velocity inside the permeable bed decays exponentially from the slip velocity on the permeable surface into the porous bed, (32b). The magnitude of this velocity also decreases as θ decreases.

Owing to percolation, wave energy is dissipated. As shown by (40c), the damping rate is given by $\mathrm{Im}(k_{11})$. In figure 4, the ratio of damping rate to wavenumber k_0 is plotted as a function of water depth, k_0h, and the depth of the thickness of the permeable bed, k_0d. It is evident that the damping rate increases as the permeable bed becomes thicker and water depth shallower. We reiterate that the real part of k_{11} is always zero and therefore the percolation does not affect the phase of the wave propagation at this order of magnitude. On the other hand, the $O(\epsilon)$ correction to the wavenumber, k_{10}, contains the real and imaginary parts as given in (45c). They are shown in figure 5. The imaginary part represents the damping rate and is independent of θ. The real part of k_{10} could be either positive or negative depending on the value of θ; k_{10} vanishes when $\theta = 1/\sqrt{2}$.

The wave-induced streaming inside the boundary layer above the permeable bed is plotted in figure 6 for $k_0h = 1.0$ and $d = 2h$ with various values of θ and β/ϵ. When θ is not zero, there is also a slip velocity along the permeable surface for the wave-

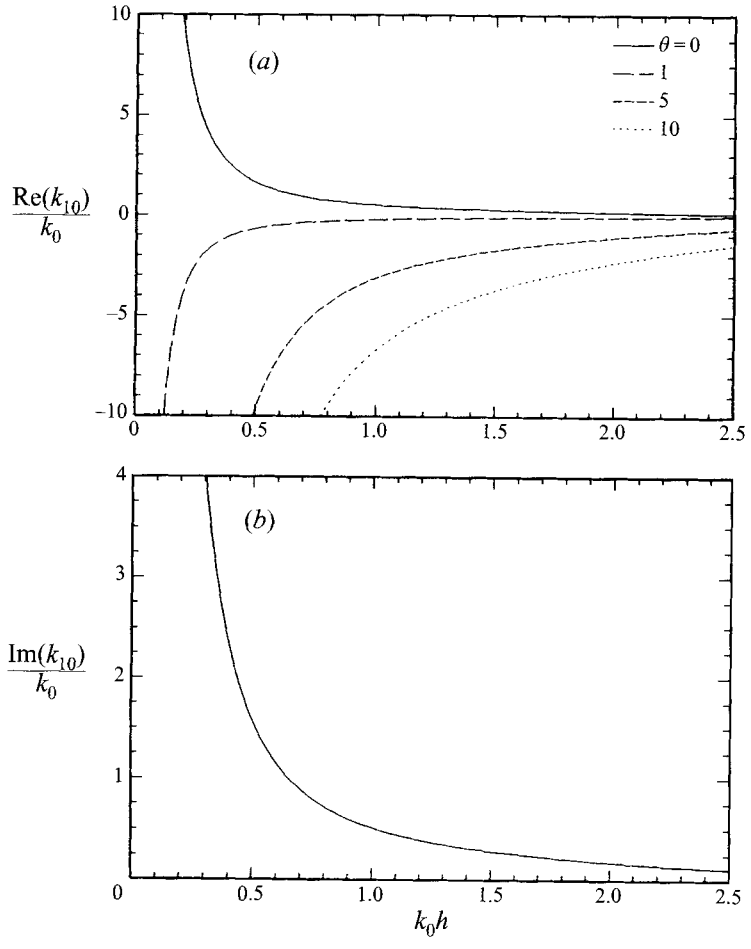

FIGURE 5. The effects of the viscous boundary layers on the wavenumber as a function of the water depth, k_0h, and the permeability parameter, θ. (*a*) The effects on the phase function and (*b*) the viscous damping rate.

induced streaming. The magnitude of the wave-induced streaming increases as the parameter β/ϵ increases. Similarly to the leading-order oscillatory velocity component the wave-induced streaming inside the porous bed also decays exponentially.

4. Comparisons between experiments and theories

In this section the experimental data for the permeable-bed cases (see tables 2 and 3) are presented and compared with theoretical results. The details of the data acquisition procedure can be found in Davis (1995).

In figure 7 the leading-order theoretical solutions and experimental data for the horizontal oscillatory velocity inside the boundary layer above the permeable bed for all cases are plotted. Laboratory data were taken along several vertical cross-sections across the wave tank; only the averaged values are plotted. The slip velocities along the permeable surface are clearly shown in the experimental data and they are consistently larger than the theoretical prediction. The overall agreement between the theoretical solutions and the laboratory data in terms of the magnitude and the profile of the oscillatory velocity inside the boundary layer is very good.

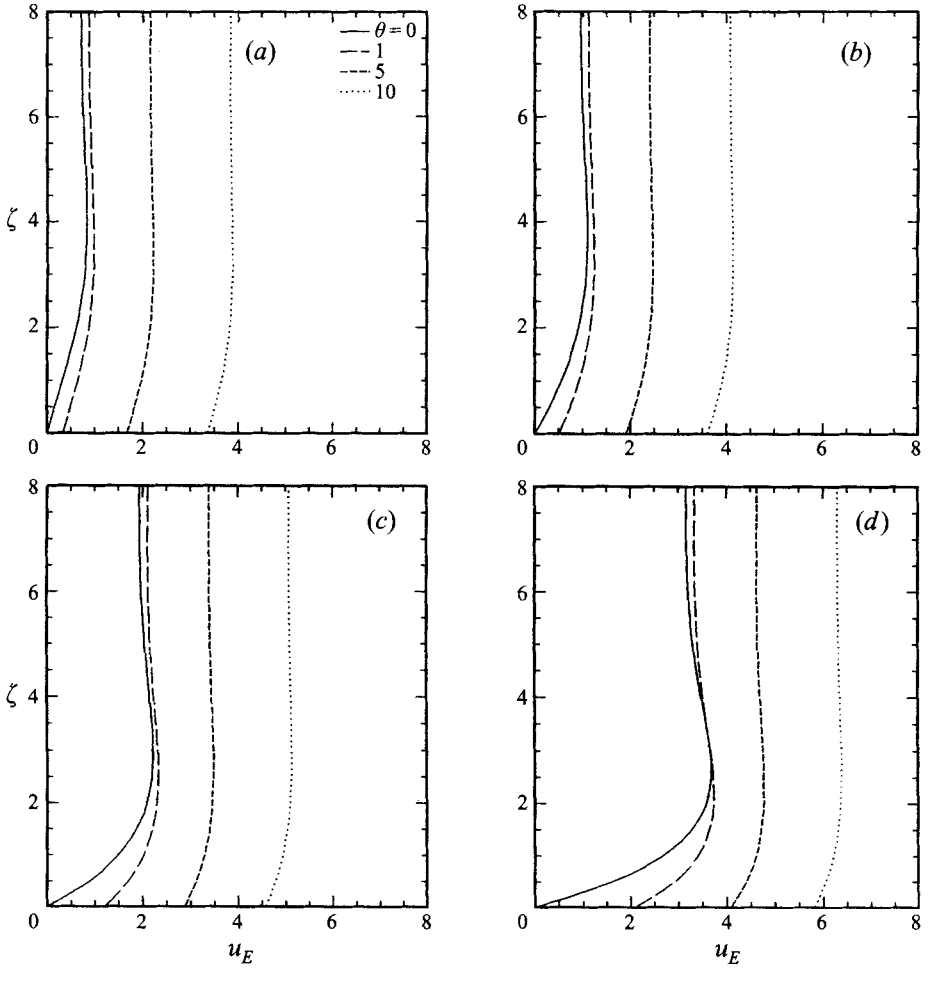

FIGURE 6. The wave-induced streaming inside the boundary layer above the permeable bed for $k_0h = 1.0$, $d = 2h$ and different values of θ and β/ϵ: (*a*) $\beta/\epsilon = 0$, (*b*) 1, (*c*) 5, (*d*) 10.

Using the physical parameters listed in tables 1 and 2, the dimensional damping coefficients, (46) and (40*c*), are calculated for the experiments and presented in table 4. The expressions for these damping coefficients are given specifically as

$$k_{10}^* = \epsilon \left(\frac{g}{\omega^2}\right) \frac{\sqrt{2}k_0^{*2}}{2k_0^*h^* + \sinh 2k_0^*h^*},$$

$$k_{11}^* = \beta \frac{2k_0^* \tanh k_0^*d}{2k_0^*h^* + \sinh 2k_0^*h^*}.$$

It is expected that the damping coefficient caused by the energy dissipation inside the Stokes boundary layer above the permeable surface remains more or less constant for all experiments. But the damping coefficient due to percolation grows quickly as the permeability increases. For the porous bed with 3 mm glass beads the energy dissipation due to percolation dominates. The free-surface elevations were measured

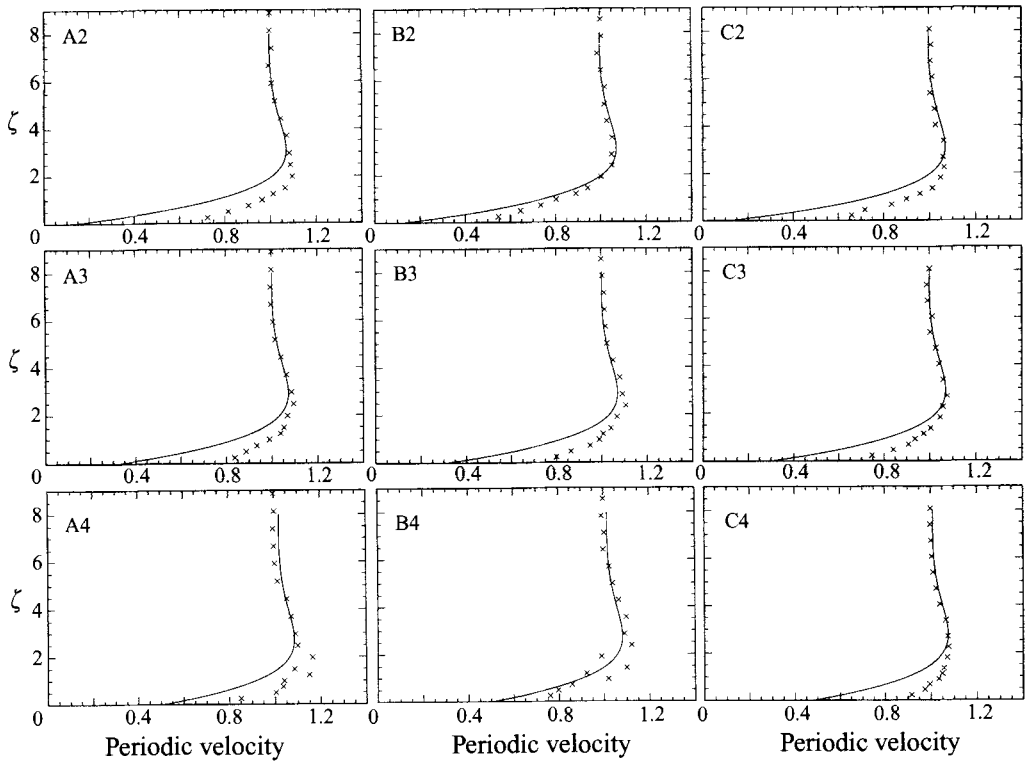

FIGURE 7. Comparison between experimental data (×) and theoretical results for the leading-order oscillatory velocity in the boundary layer above the permeable bed. Labels refer to the experimental parameters listed in table 3.

Exp.	k_{10}^* (10^{-3} m^{-1})	k_{11}^* (10^{-3} m^{-1})	$k_{10}^* + k_{11}^*$ (10^{-3} m^{-1})
A2	3.58	2.67	6.25
A3	3.58	15.82	19.41
A4	3.58	65.45	69.03
B2	2.61	1.72	4.33
B3	2.60	13.17	15.77
B4	2.60	54.47	57.08
C2	2.44	1.68	4.12
C3	2.43	12.88	15.31
C4	2.44	53.36	55.80

TABLE 4. Dimensional damping coefficients for experiments over a permeable bottom.

along the porous bed ($0 < x < 1.82$ m) with 5 cm increments. Taking the damping and the reflection into consideration, the wave profile over the porous bed can be expressed as follows:

$$\eta(x,t) = a_1 \cos(kx - \omega t)\mathrm{e}^{-\kappa x} + Ra_1 \cos(kx + \omega t + \lambda_0)\mathrm{e}^{-\kappa(2l-x)},$$

in which κ is the total damping coefficient, R the reflection coefficient caused by the porous bed, $l = 1.82$ m the length of the porous bed and λ_0 a phase constant. The

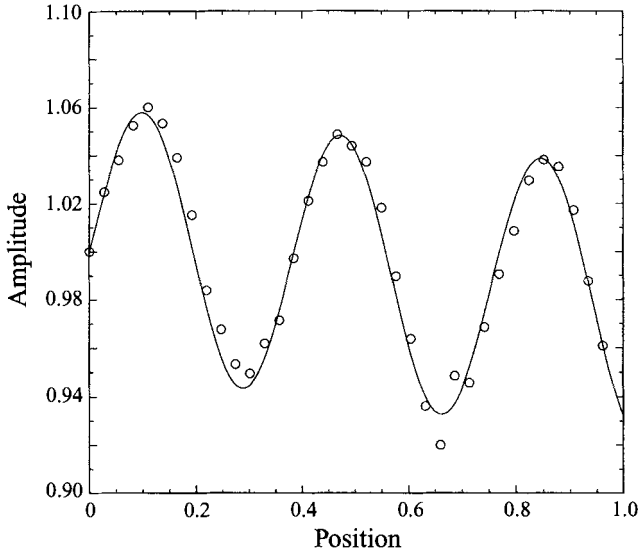

FIGURE 8. Wave envelope over the porous bed for experiment C3. The solid line is the theoretical result and the circles are experimental data.

experimental data for the wave envelope over the porous bed is plotted in figure 8 for experiment C3. The reflection coefficient is estimated as $R = 5.7\%$. Using the theoretical solution for the damping coefficient, i.e. $\kappa = k_{11}^* + k_{10}^*$, the theoretical wave envelope is also plotted in the same figure. The agreement between the experimental data and theory is good. Similar results are also obtained for different experiments (Davis 1995).

In figure 9 the wave-induced streaming is plotted. The differences between the experimental data and theoretical solutions are quite large, especially for the cases of large glass beads (i.e. larger permeability). Similar to the solid-bottom case (see figure 2), the laboratory data near the outer edge of the boundary layer are always much smaller than the theoretical predictions. We speculate that a weak circulation pattern exists in the wave tank, generated by other physical mechanism, which has the same order of magnitude of the wave-induced streaming. The higher-order effects might also play a role (Sleath 1972). Nevertheless, the experimental data demonstrate that the steady streaming does increase as the permeability of the permeable bed increases.

5. Concluding remarks

A perturbation theory has been developed for flow motions in the boundary layers adjacent to a permeable bed. The theory is based on the assumptions of small wave amplitude, weak permeability, and small viscosity. Both the oscillatory velocity component and the wave-induced streaming are calculated from the perturbation theory. Theoretical results are compared with the laboratory data; reasonable agreement is observed for the oscillatory velocity component. The theory tends to over-predict the wave-induced streaming as compared with the experimental data. Both theoretical and experimental data indicate that the permeable bed causes the slip velocity in both oscillatory and steady velocity components. Moreover, the wave-induced streaming

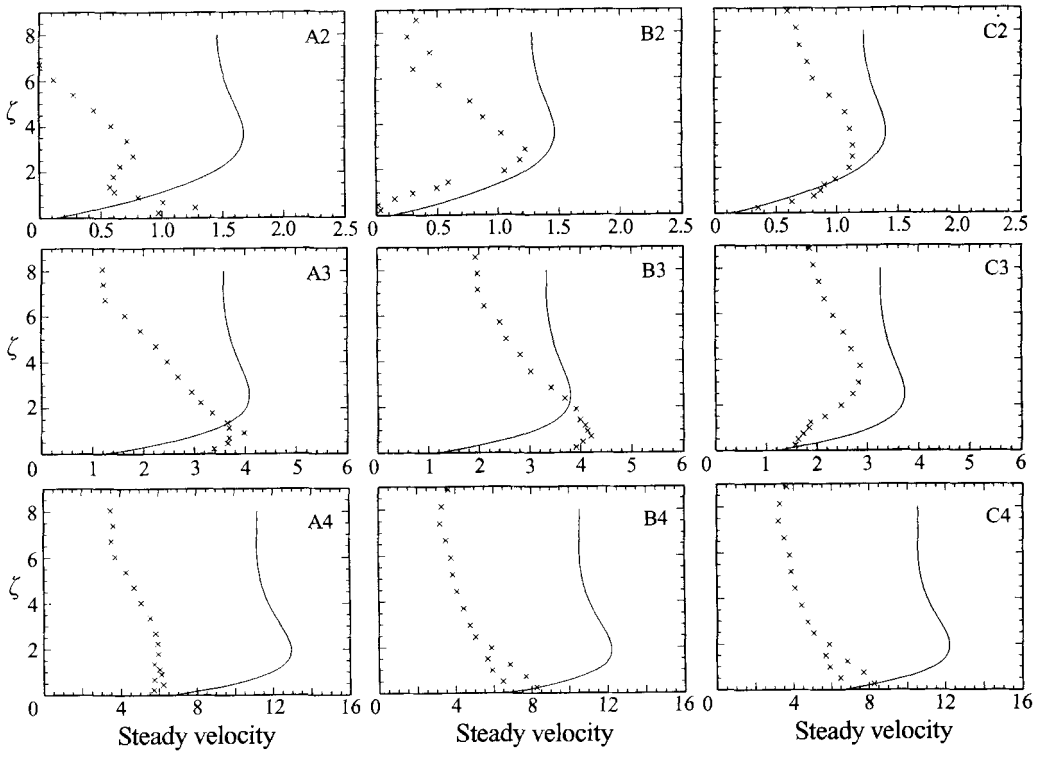

FIGURE 9. Comparison between experimental data and theoretical results for the wave-induced streaming in the boundary layer above the permeable bed.

increases with increasing permeability. The theory also provides the damping rate due to dissipation in viscous boundary layers and in the permeable bed.

In studying Poiseuille flows over a permeable wall, Beavers & Joseph (1967) proposed a slip boundary condition along the permeable surface. Using our notation, the slip boundary condition can be expressed as

$$\frac{\partial u^{+*}}{\partial z^*} = \frac{\Gamma}{K^{1/2}}(u^{+*} - u^{-D*}), \tag{58}$$

along $z^* = -h^*$, where Γ is a dimensionless parameter. Using the theory developed herein, we find that

$$\Gamma = \left(\frac{K}{\gamma}\right)^{1/2}, \tag{59}$$

which depends only on the structure of the permeable bed and is consistent with Beavers & Joseph's original hypothesis. We reiterate here that the slip condition, (58) and (59), is extended from the steady Poiseuille flows to the present oscillatory boundary layer flows. It cannot be applied to the wave-induced streaming directly.

Since the wave-induced streaming is a second-order quantity and can be confused with the existing second-order currents in the wave tank, the U-shaped oscillatory flume facility may be considered as an alternative for future laboratory experiments. Moreover, different permeable materials perhaps should be used for determining the parameter γ.

This research was, in part, supported by a research grant from the National Science Foundation (CTS-8902407) and by the New York Sea Grant research Institute. Dr J. Wen assisted in preparing the figures presented in this paper.

REFERENCES

BATCHELOR, G. K. 1967 *An Introduction to Fluid Dynamics.* Cambridge University Press.

BATCHELOR, G. K. 1974 Transport properties of two-phase materials with random structure. *Ann. Rev. Fluid Mech.* **6**, 227–255.

BEAVERS, G. S. & JOSEPH, D. D. 1967 Boundary conditions at a naturally permeable wall. *J. Fluid Mech.* **30**, 197–207.

BEECH, N. W. 1978 Laser Doppler measurements in the oscillatory boundary layer beneath water waves. *DSIA Elektronik* No. 23, September.

BRINKMAN, H. C. 1947 On the permeability of media consisting of closely packed porous particles. *Appl. Sci. Res.* **A1**, 81–86.

CARTER, T. G., LIU, P. L.-F. & MEI, C. C. 1973 Mass transport by waves and offshore sand bedforms. *J. Waterways, Harbor, Coastal Engineering Div., ASCE* **99**, 165–184.

DAGAN, G. 1979 The generalization of Darcy's law for nonuniform flows. *Water Resources Res.* **15**, 1–7.

DAVIS, M. H. 1995 Water wave-induced streaming in the bottom boundary layer over a permeable bed. MS thesis, School of Civil and Environmental Engineering, Cornell University.

DOWNING, S. L. 1993 Measurements of the velocity structure in the bottom boundary layer under ocean waves. MS thesis, Department of Physics, Cornell University.

HAPPEL, J. & BRENNER, H. 1985 *Low Reynolds Number Hydrodynamics.* Prentice-Hall.

HOWELLS, I. D. 1974 Drag due to the motion of Newtonian fluid through a sparse random array of small fixed rigid objects. *J. Fluid Mech.* **64**, 449–475.

HWUNG, H. H. & LIN, C. 1990 The mass transport of wave propagating on a slopping bottom. *22nd Conf. Coastal Engng*, pp. 544–556.

LIU, P. L.-F. 1973 Damping of water waves over a porous bed. *J. Hydraulic Engng, ASCE* **99**, 2263–2271.

LIU, P. L.-F. 1977 Mass transport in water waves propagated over a permeable bed. *Coastal Engng* **1**, 79–96.

LIU, P. L.-F. & DALRYMPLE, R. A. 1984 The damping of gravity waves due to percolation. *Coastal Engng* **8**, 33–49.

LONGUET-HIGGINS, M. S. 1953 Mass transport in water waves. *Phil. Trans. R. Soc. Lond.* A **245**, 535–581.

LUNDGREN, T. S. 1972 Slow flow through stationary random beds and suspensions of spheres. *J. Fluid Mech.* **51**, 273–299.

PUTNAM, J. A. 1949 Loss of water wave energy due to percolation in a permeable sea bottom. *Trans. Am. Geophys. Union* **30**, 349–356.

REID, R. O. & KAJIURA, K. 1957 On the damping of gravity waves over a permeable sea bed. *Trans. Am. Geophys. Union* **38**, 362–666.

RUSSELL, R. C. H. & OSORIO, J. D. C. 1957 An experiment investigation of drift profiles in a closed channel. *Proc. 6th Conf. Coastal Engng, ASCE*, pp. 171–193.

SKJELBREIA, J. E. 1987 Observations of breaking waves on slopping bottoms by use of laser doppler velocimetry. *W. M. Keck Laboratory of Hydraulics and Water Resources, Caltech., Rep.* KH-R-48.

SLEATH, J. F. A. 1972 A second approximation to mass transport by water waves. *J. Marine Res.* **30**, 295–304.

SLEATH, J. F. A. 1978 Discussion of "Mass transport in water waves propagated over a permeable bed" (by P.L.-F. Liu). *Coastal Engng* **2**, 169–171.

SLEATH, J. F. A. 1984 Measurements of mass transport over a rough bed. *19th Conf. Coastal Engng*, pp. 1149–1160.

STOKES, G. G. 1847 On the theory of oscillatory waves. *Trans. Camb. Phil. Soc.* **8**, 441–455.

TAM, C. K. W. 1969 The drag on a cloud of spherical particles in low Reynolds number flow. *J. Fluid Mech.* **38**, 537–546.